



Final Year Research Report

SUNLINK II: Light-Based Wireless Communication Using Sunlight

Ryan Farrell

Co-worker: Vivek Chauhan
Supervisor: Talia Xu

Department of Electrical, Computer, and Software Engineering
The University of Auckland

October 2025

ABSTRACT

Ambient light offers a vast and renewable resource that can be harnessed for wireless communication, presenting a promising alternative to conventional radio frequency methods. By using the sun as a near-infinite light source, visible light communication (VLC) systems have the potential to enable sustainable, low-power Internet of Things (IoT) networks capable of operating in remote or energy-constrained environments. This research investigated the feasibility of a sunlight-based backscatter communication system that incorporates dynamic sun tracking to maximise signal reliability. The system comprised two main subsystems: a light sensing and tracking module, and a communication module. The tracking module employed a dual light sensor array with motorised control to follow a moving light source. Results showed that while the system could accurately detect light direction, the sensors exhibited oversaturation under high-intensity illumination, and the motor's average power consumption of approximately 1 W per 90° rotation was deemed unfeasible for low-power IoT applications. The communication subsystem demonstrated the ability to transmit and detect modulated light signals over a maximum range of 1.5m under ambient conditions, with signal strength decreasing exponentially with distance. These findings highlight key design limitations, including insufficient illumination strength and the need for more advanced modulation and decoding methods. Overall, the study reinforces the potential of sunlight as a communication medium but reveals that practical implementation requires substantial refinement in both motor tracking efficiency and communication range to achieve a viable, low-power VLC solution for future IoT systems.

DECLARATION

Student

I hereby declare that:

1. This report is the result of the final year project work carried out by my project partner (see cover page) and I under the guidance of our supervisor (see cover page) in the 2025 academic year at the Department of Electrical, Computer and Software Engineering, Faculty of Engineering, University of Auckland.
2. This report is not the outcome of work done previously.
3. This report is not the outcome of work done in collaboration, except that with a potential project sponsor (if any) as stated in the text.
4. This report is not the same as any report, thesis, conference article or journal paper, or any other publication or unpublished work in any format.

In the case of a continuing project, please state clearly what has been developed during the project and what was available from previous year(s):

Signature: R.Farrell

Date: 18/10/2025

ACKNOWLEDGEMENT

I would like to express my sincere gratitude to my supervisor, Talia Xu, for her guidance, support, and valuable feedback throughout the duration of this project. Her insights and encouragement have been instrumental in shaping the outcome of this work.

I would also like to thank my project partner, Vivek Chauhan, for his collaboration, effort, and shared commitment to achieving our project goals. Working alongside him made this project both productive and enjoyable.

A special thanks goes to Felix Marattukalam for his technical assistance and support in sourcing components and helping with laboratory logistics.

Finally, I would like to thank my family and friends for their ongoing support, patience, and encouragement throughout my studies and this project.

TABLE OF CONTENTS

ABSTRACT	i
DECLARATION	ii
ACKNOWLEDGEMENT	iii
TABLE OF CONTENTS	iv
LIST OF FIGURES	vi
List of Figures	vi
LIST OF TABLES	vii
List of Tables	vii
GLOSSARY	viii
1 INTRODUCTION	1
1.1 Research Aim	1
1.2 Research Objectives	1
2 LITERATURE REVIEW	2
2.1 Introduction to IoT Wireless Communication	2
2.2 Visible Light Communication: An Emerging Alternative	3
2.3 Passive Visible Light Communication Systems	3
2.4 Leveraging Sunlight for Optical Communication	5
2.5 Research Gaps and Future Directions	6
3 EXPERIMENTAL METHODS	6
3.1 Dynamic Sun-Tracking Subsystem	7
3.1.1 Sun-Tracking System Design	7
3.1.2 Test Setup and Methods	7
3.2 Communication Subsystem	8
3.2.1 Transmitter and Receiver Design	8
3.2.2 Test Equipment	9
3.2.3 Test Methods and Environment Conditions	10
4 RESULTS	11
4.1 Dynamic Sun-Tracking Subsystem	11
4.1.1 Light Sensing Array	11
4.1.2 Motor Circuit	12
4.2 Communication Subsystem	14
4.2.1 Pure Noise Signal	14
4.2.2 Distance 0.2m	14
4.2.3 Distance 0.5m	14
4.2.4 Distance 1.0m	15
4.2.5 Distance 1.5m	15

4.2.6	Graphs	16
5	DISCUSSIONS	17
5.1	Light Sensing Array	17
5.2	Motor Application	18
5.3	Communication System	18
6	CONCLUSIONS	20
7	RECOMMENDATIONS FOR FUTURE WORKS	21
References		22
A Sun-Tracking Subsystem LTSpice Models		24

LIST OF FIGURES

List of Figures

1	NZ Radio spectrum allocations as of 2025.	2
2	Flow diagram of full motor control loop.	7
3	Testing setup for light sensing array.	8
4	Communication subsystem block diagram.	10
5	Voltage versus angular position for the light-sensing array at four illumination levels: 100% (top left), 75% (top right), 50% (bottom left), and 10% (bottom right). PD_Voltage_V represents the measured photodiode voltage, and LDR_Voltage_V represents the measured LDR array voltage.	11
6	Graph showing the illumination levels in Lux vs angle of sensor for the 10%, 50%, 75% and 100% light levels used in the experiment.	12
7	LTS spice simulation result for the NEMA 17 stepper motor showing current response to an applied step input signal.	13
8	Oscilloscope output for pure noise signal, in (left) daylight ambient conditions and (right) dark light conditions.	14
9	Oscilloscope output for measurement taken at 0.2m, in (left) daylight ambient conditions and (right) dark light conditions.	15
10	Oscilloscope output for measurement taken at 0.5m, in (left) daylight ambient conditions and (right) dark light conditions.	15
11	Oscilloscope output for measurement taken at 1.0m, in (left) daylight ambient conditions and (right) dark light conditions.	16
12	Oscilloscope output for measurement taken at 1.5m, in (left) daylight ambient conditions and (right) dark light conditions.	16
13	Bar graph showing decreasing maximum voltage with increased distance (left) and line graph showing downward trend with increased distance (right)	17

LIST OF TABLES

List of Tables

- | | | |
|---|--|----|
| 1 | Summary of measured results from the experiments performed on the motor.
Note that the voltages and currents stated in the bottom three rows (covering
the 0-270° sweep) are averages for both the measured and simulated results. . . | 13 |
|---|--|----|

GLOSSARY

Acronym / Abbreviation	Full Description
ADC	Analog-to-Digital Converter
ASCII	American Standard Code for Information Interchange
DC	Direct Current
FFT	Fast-Fourier Transform
FoV	Field of View
FSK	Frequency Shift Keying
GPIO	General-Purpose Input/Output
Hz	Hertz (cycles per second)
IoT	Internet of Things
LCD	Liquid Crystal Display
LED	Light Emitting Diode
LDR	Light Dependent Resistor
LoS	Line of Sight
LTSpice	Linear Technology SPICE
Lux	Unit of illuminance
kLux	A Thousand Lux
mA	Milliampere
MOSFET	Metal-Oxide-Semiconductor Field-Effect Transistor
mV/div	Millivolt per Division (oscilloscope voltage scale)
OOK	On-Off Keying
PD	Photodiode
PI	Proportional–Integral (control algorithm)
PWM	Pulse Width Modulation
RF	Radio Frequency
SNR	Signal-to-Noise Ratio
TIA	Transimpedance Amplifier
VLC	Visible Light Communication
W	Watt (unit of measurement for power)
mW	Milli-Watt (thousandth of a Watt)

1 INTRODUCTION

Visible Light Communication (VLC) is an emerging technology that uses light for low-power wireless data transmission. This method, in its passive form, is particularly suited for Internet of Things (IoT) and remote sensing applications where energy efficiency is critical. Among potential light sources, sunlight offers a sustainable and naturally available medium but introduces challenges due to its directionality and changing intensity throughout the day.

This project investigates the use of sunlight as a transmission medium for a low-power, multi-sensor communication system. Unlike systems that rely on artificial or ambient indoor light, this approach aims to achieve consistent and efficient performance in real outdoor conditions. To address the variability of sunlight, research was conducted into the use of a motor-driven sun-tracking mechanism designed to maintain optimal alignment and maximise reflected light for data transmission.

This research seeks to overcome the inherent limitations of current ambient light communication systems, which are hindered by noise, interference, and fluctuating performance under variable environmental conditions. By developing a self-aligning, sunlight-based communication system, the project aims to demonstrate a scalable and energy-efficient solution for sustainable IoT networks and remote sensing applications where RF communication is impractical or power-constrained.

1.1 Research Aim

To design and prototype a communication system that utilises sunlight as a medium for backscattered communication, incorporating dynamic sun tracking to maximise signal reliability.

1.2 Research Objectives

- Review existing VLC technologies to understand their operation, limitations, and applications.
- Identify performance limitations in ambient light based systems and consider potential improvements.
- Design and implement a sun-tracking subsystem using motor control to maintain solar alignment.
- Design and prototype a point-to-point communication subsystem using light based modulation for data transmission.
- Evaluate system performance under varying lighting conditions and compare with existing ambient light alternatives.

- Assess the scalability and feasibility of the system for low-power IoT and remote sensing applications.

2 LITERATURE REVIEW

2.1 Introduction to IoT Wireless Communication

Wireless communication has undergone substantial evolution since the early development of radio technology. The emergence of radio communication in the late 19th and early 20th centuries laid the path for modern wireless systems, enabling the transmission of information between points without any physical connections [1]. As wireless technologies evolved, there has been a continuous push toward increasing data rates, reliability, and energy efficiency. Traditional radio frequency (RF) communication systems are widely distributed for applications ranging from mobile networks to satellite communication, but they face inherent limitations due to spectrum scarcity, regulatory constraints, and interference [2]. Figure 1 illustrates the RF spectrum allocations for New Zealand, emphasizing the increasing congestion and demand for alternative wireless channels [3].

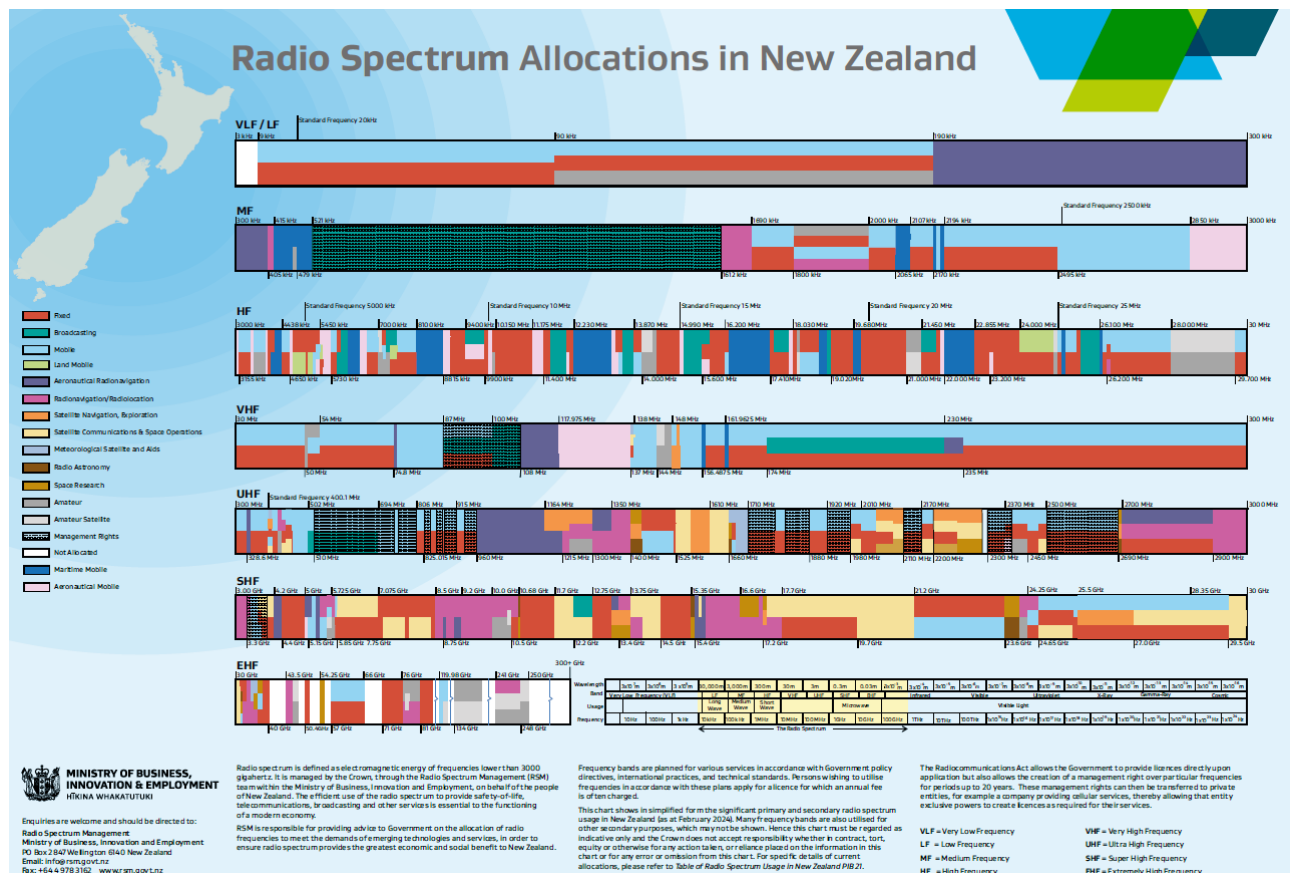


Figure 1: NZ Radio spectrum allocations as of 2025.

Visible Light Communication (VLC) has emerged as a promising wireless technology capable of addressing several limitations of traditional RF systems. VLC utilises light waves within the

visible spectrum to transmit information, providing a vast unlicensed bandwidth and strong immunity to electromagnetic interference, making it suitable for environments where RF congestion or interference is problematic. Unlike RF-based systems, VLC offers secure, localised communication confined to illuminated regions, improving spatial reuse and reducing signal leakage. VLC is particularly well suited for IoT applications, especially in its passive form, where data transmission occurs without the need for active light emission. Instead, ambient light is reflected and modulated towards the receiver, significantly reducing overall power consumption.

Exploring VLC as an alternative to traditional RF communication presents a promising pathway toward wireless low-power data exchange for remote IoT applications.

2.2 Visible Light Communication: An Emerging Alternative

Visible Light Communication (VLC) exploits the visible portion of the electromagnetic spectrum (roughly 400-700 nm) to transmit data by modulating light sources, typically LEDs, and detecting them using photodiodes or image sensors [4]. Unlike RF systems, VLC can use existing lighting infrastructure both to illuminate a space and to serve as communication channels [5]. For Internet of Things (IoT) applications, VLC presents distinct advantages. Its capacity to reuse existing lighting infrastructure aligns with the design goals of low-cost and energy-efficient connectivity. Since VLC transmitters can be integrated into LED lighting, and receivers implemented with low-cost photodiodes, deployment costs can be minimized.

Despite these benefits, VLC systems face several challenges. Performance depends strongly on line-of-sight conditions, as obstacles or misalignment between transmitter and receiver can severely degrade link reliability. Additionally, ambient illumination, such as sunlight or fluorescent lighting, introduces optical noise that may reduce signal-to-noise ratio and limit achievable data rates. These constraints motivate the exploration of novel architectures that extend VLC's applicability beyond traditional active LED transmitters.

One promising direction is the development of passive VLC systems, which eliminate the need for dedicated light sources. Instead, these systems modulate or reflect ambient light, either natural or artificial, to convey data. Such approaches are particularly well suited for ultra-low-power IoT systems, where minimizing energy consumption is critical, and can enable communication between devices without the need for a power-intensive emitter.

2.3 Passive Visible Light Communication Systems

As the field of Visible Light Communication continues to advance, research focus has increasingly shifted toward passive VLC - a paradigm that exploits existing ambient light sources to enable ultra-low-power data transmission. Rather than relying on active emission sources,

passive VLC systems utilize reflected or modulated ambient light to convey information. This approach aligns closely with the growing need for sustainable, energy-efficient communication methods in Internet of Things (IoT) applications, where minimizing power consumption and hardware complexity are critical. By leveraging freely available light in the environment, passive VLC offers a pathway toward scalable, battery-free connectivity between low-power devices.

One of the pioneering works in this field, *Passive Communication with Ambient Light* by Wang et al. [6], introduced the concept of modulating ambient light through reflective surfaces, thereby eliminating the need for direct control over the light source. In their study, sequences of reflective materials were attached to moving objects such as vehicles, enabling these surfaces to encode data that could be decoded by a stationary photodiode receiver. The system's performance was found to depend heavily on the receiver's Field of View (FoV) and the distance to the reflective object. A wider FoV improved spatial coverage but increased signal interference, while greater separation between the transmitter and receiver reduced overall signal strength. These limitations in range and sensitivity motivated further research into more adaptable and energy-efficient passive VLC architectures.

Continuing the theme of passive communication for mobile objects, Wang et al. [7] proposed a novel infrastructure-to-vehicle (I2V) communication system, dubbed RetroI2V, which repurposes conventional retro-reflective road signs as passive transmitters. The system enables these signs to convey data to vehicles without compromising their original functionality as traffic indicators. RetroI2V functions as a visible light backscatter communication system, in which a vehicle's own headlights act as the illumination source while the retro-reflective surface serves as a passive modulator. Due to physical characteristics of retro-reflectors, the incident light is directed back along its incoming path, returning towards the vehicle. To ensure stable communication and eliminate visible flicker, a key consideration for VLC applications, RetroI2V employed late polarization modulation, a technique that allows high-frequency intensity variations without perceptible changes to human observers. Experimental evaluation demonstrated that the system achieved reliable communication at distances of up to 101 meters, highlighting its potential for long-range, low-cost I2V connectivity.

Also utilising retro-reflective properties and an LCD shutter, PassiveVLC [8] shifts focus towards low-power, battery-free IoT applications by modulating ambient light by selectively reflecting or blocking incident light from existing illumination sources, backscattering data without the need for an active light emitter. Using on-off keying (OOK) for simplicity and efficiency, the system demonstrates reliable data transmission over several meters with only microwatts of power consumption. As is the case for all VLC systems, its performance is limited by line-of-sight requirement and environmental variability, prompting further research into more adaptive and robust passive VLC designs. Overall, PassiveVLC represents an important step

toward practical, scalable visible-light backscatter communication for low-power IoT devices.

2.4 Leveraging Sunlight for Optical Communication

Building on the concept of passive optical communication, recent research has explored leveraging sunlight as a naturally available illumination source for data transmission. This shift is driven by the growing demand for ultra-low-power communication, a key requirement in many IoT applications, as sunlight-based systems eliminate the need for dedicated light sources while maintaining sustainable and efficient operation.

One of the more successful projects in this area, LuxLink [9], demonstrated a significant advancement in low-power sunlight-based communication, achieving an operational range of 4 -60m under outdoor conditions - far exceeding the capabilities of earlier systems. The design employed liquid crystal display (LCD) shutters to modulate the intensity of incident sunlight and simple photodiodes as receivers. By adopting frequency shift keying (FSK) modulation, LuxLink enabled flicker-free data transmission that remained compatible with low-cost photodiode detection. This marked a substantial improvement over earlier pulse-based modulation methods, which inherently produced perceptible flickering.

Sol-Fi, presented by Tapia et al. [10], introduces a system designed to deliver both illumination and data communication in indoor environments using sunlight as the optical carrier. The system employs commercial sunlight collectors and optical fibres to channel sunlight indoors, where a custom transmitter encodes data onto the light beam. On the transmitter side, Sol-Fi explores the use of both liquid crystal (LC) shutters and digital micromirror devices (DMDs) for modulation. Furthermore, the system's optical architecture supports either full-spectrum modulation or spectral band division, allowing different portions of the spectrum to carry independent data streams. Experimental evaluation demonstrated that, depending on the number of spectral bands and the chosen modulator type, data rates up to 80 kbps could be achieved over distances of up to 5 meters, with an FoV ranging between 30° and 60°.

PassiveCam [11], presented by Ghiasi et al., leverages the emerging technology of transparent screens, transforming windows into interactive displays. Unlike traditional systems that rely on LEDs, PassiveCam operates entirely using ambient light, eliminating the need for an active light source. In contrast to passive VLC systems that employ photodiodes or phototransistors at the receiver, PassiveCam builds on screen-to-camera communication by using a smartphone camera and software to receive and decode the displayed information. The system modulates a video signal on the screen such that it remains imperceptible to the human eye but can be captured by a camera, enabling multiple users to receive the information simultaneously. Notably, the LCD is powered by sunlight rather than an LED backlight, which typically accounts for approximately 80% of display power consumption, significantly reducing energy requirements.

2.5 Research Gaps and Future Directions

Despite significant advancements in passive visible light communication, several critical limitations remain that constrain its deployment for low-power IoT applications in remote or energy-constrained environments. Existing systems, such as RetroI2V [7], and PassiveVLC [8], demonstrate the potential for ambient-light-based data transmission; however, their reliance on controlled illumination, limited communication range, or line-of-sight constraints restricts practical applicability. Systems like LuxLink [9] and Sol-Fi [10], which utilize sunlight or ambient light, have further illustrated the promise of energy-efficient communication, but they remain limited in terms of practical range, field-of-view, and robustness under variable environmental conditions. Furthermore, many current designs focus on proof-of-concept demonstrations in laboratory or controlled outdoor settings, with little attention to autonomous operation in remote IoT scenarios, where maintenance and power availability are highly constrained.

These limitations suggest a clear opportunity for research into scalable, low-power passive VLC systems that utilise sunlight as a naturally occurring source of illumination. By incorporating sunlight tracking and adaptive modulation strategies, devices could maintain optimal alignment with the light source, maximizing communication reliability while minimizing power consumption. Such approaches would enable fully autonomous IoT nodes capable of sustaining long-term operation without additional energy input (i.e. changing batteries), a key requirement for remote sensing and environmental monitoring applications.

The work proposed in this project aims to address these gaps by developing a sunlight-powered, passive communication system capable of reliable device-to-device transmission using ambient light. The proposed design demonstrates a pathway toward energy-efficient, sustainable communication for IoT networks in remote environments. By exploring novel techniques in sunlight harvesting and optical modulation, this research contributes toward practical, deployable passive VLC systems that could overcome the key limitations of existing approaches and expand the applicability of visible light communication in remote IoT scenarios.

3 EXPERIMENTAL METHODS

This section describes the experimental setup used for the project, which aimed to evaluate the performance and feasibility of both major subsystems - the communication subsystem and the dynamic sun-tracking subsystem. Each was tested independently under controlled laboratory conditions to characterise signal performance, environmental robustness, and power efficiency. The communication subsystem experiments focused on assessing optical signal strength and transmission range under varying ambient light levels, while the sun-tracking subsystem experiments assessed the accuracy of the light-sensing array and the mechanical power requirements of the motor. Together, these tests provided a comprehensive assessment of the system's func-

tionality and validated its design objectives.

3.1 Dynamic Sun-Tracking Subsystem

3.1.1 Sun-Tracking System Design

The proposed dynamic sun-tracking subsystem consists of a light-sensing array, control electronics, and two motors configured for azimuth and elevation movement. The light-sensing circuit comprises four Light Dependent Resistors (LDRs) arranged in a 2x2 grid spaced 3cm apart, with two additional photodiodes positioned at the centre to provide fine-resolution light intensity measurements. Each LDR forms a voltage divider with a fixed resistor, producing an analogue voltage proportional to incident light, which is digitized via the 10-bit ADC of an MSP430 microcontroller.

A Proportional–Integral (PI) control algorithm implemented on an Arduino UNO R4 calculates differential voltages from the sensor array to determine horizontal and vertical tracking adjustments. These outputs drive the azimuth motor, a NEMA 17 stepper motor controlled via an A4988 driver on a 12 V supply, and the elevation motor, which was not implemented in the experimental design, a 28BYJ-48 geared motor controlled via a ULN2003 motor driver, on a 5 V supply. The azimuth motor employs step/direction control with 1/16 micro stepping, while the elevation motor uses a 4-step sequence control. This setup allows the system to dynamically align toward the brightest light source. Figure 2 shows the full motor control loop.

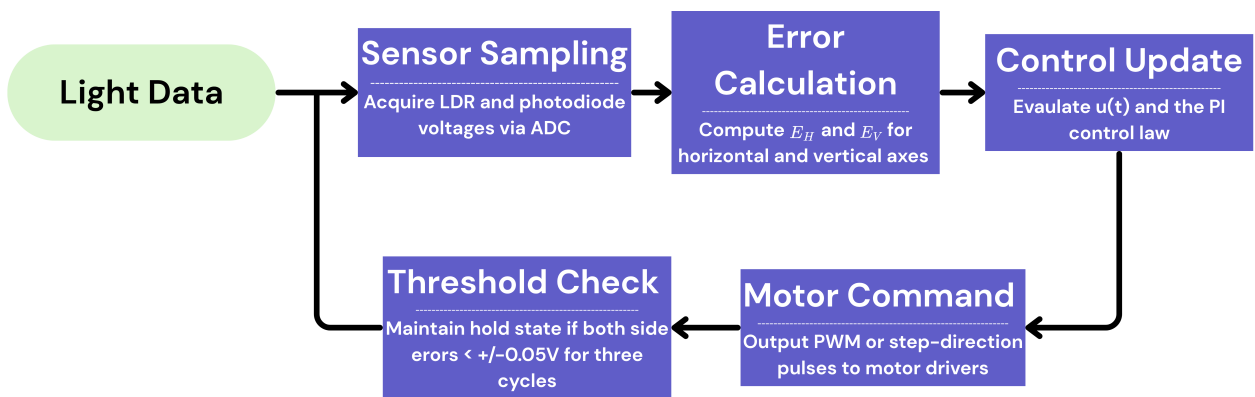


Figure 2: Flow diagram of full motor control loop.

3.1.2 Test Setup and Methods

Experiments on the dynamic sun-tracking subsystem were conducted indoors under controlled illumination to emulate sunlight conditions. The testing was carried out as two distinct experiments. The first experiment focused on evaluating the light-sensing array (LDRs and photodiodes). The array was illuminated using a 10 W LED torch in a fixed position at four relative brightness levels: 10%, 50%, 75%, and 100%. Light intensity was measured with a phone-based lux meter for reference. Motor control movement was emulated by manually rotating the sensor

array in 30° segments to either side of the light source, following a 270° total range. Differential voltages from the sensor array were measured by the ADC of the MSP430 microcontroller in a range between 0-5V to determine the optimal alignment angle. A reading near 5V indicated maximum light alignment. The setup, including the relative range of the light source, sensor array, and signal chain, is illustrated in Figure 3.

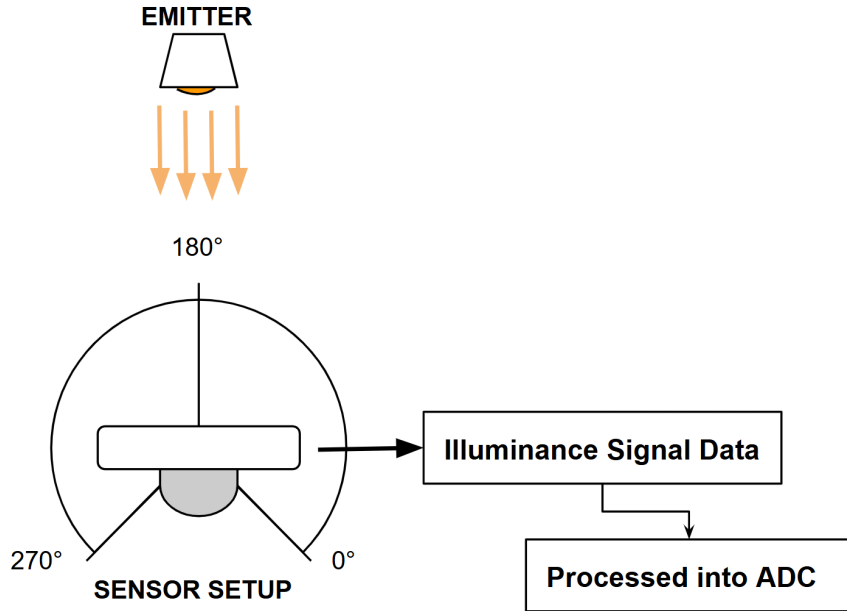


Figure 3: Testing setup for light sensing array.

The second experiment evaluated the motor performance and power draw independently of the light-sensing array. The azimuth motor was driven through a sequence of discrete steps covering $0\text{--}90^\circ$, $0\text{--}180^\circ$, and $0\text{--}270^\circ$, and measurements of voltage and current were recorded for idle and single-step operation using a Keysight multimeter. This test assessed the motor's power draw and efficiency, and hence feasibility across the full range of motion.

Initial step-response simulations of the azimuth motor were performed in LTSpice (see Appendix A for the LTSpice model), and the simulation results are compared with the measured voltages and currents in the results section.

3.2 Communication Subsystem

3.2.1 Transmitter and Receiver Design

The communication subsystem consists of a transmitter and a receiver designed to provide a proof-of-concept of a visible light communication link. The transmitter is controlled by an MSP430 microcontroller using a discrete Frequency Shift Keying (FSK) modulation scheme with 5-bit repetition coding. In this configuration, a binary '0' is represented by five pulses at 170 Hz (f_0), and a binary '1' by five pulses at 230 Hz (f_1). These carrier frequencies were selected to be high enough to eliminate visible flicker, an important consideration in VLC

systems to prevent discomfort for humans and animals, yet low enough to maintain adequate signal quality within the bandwidth constraints of the receiver circuit. The 5-bit repetition approach simplifies decoding and increases reliability by reducing the probability of bit errors, at the cost of data rate - a trade-off considered acceptable for the intended low-power IoT application.

ASCII encoding was used for message representation. While the encoding format does not influence signal quality, its fixed 7-bit character length simplifies bit-rate calculations and reduces firmware complexity.

Because the GPIO output of the MSP430 is limited to 0–3.3 V logic levels, a MOSFET-based driver circuit was employed to amplify the signal to 0–5 V, ensuring sufficient modulation depth across the LCD element. The LCD, repurposed from a pair of commercial 3D glasses, acts as a light shutter, modulating the intensity of the incident light beam according to the output of the MOSFET driver.

On the receiver side, a photodiode detects the modulated light. The resulting photocurrent is first converted to a measurable voltage using a transimpedance amplifier (TIA) stage. The amplified signal then passes through a band-pass filter with a 160–240 Hz passband, designed to isolate the transmitted FSK frequencies while rejecting low-frequency noise and ambient-light variations. The receiver circuit was originally intended to interface with the ADC input of a second MSP430 microcontroller for digital decoding. However, due to technical difficulties, only oscilloscope measurements were captured during testing. Although this prevented full end-to-end validation of the communication link, the observed waveforms were deemed sufficient to evaluate system performance and infer the feasibility of successful message decoding.

3.2.2 *Test Equipment*

The experimental setup used to test the communication subsystem is illustrated in Figure X. Two separate breadboard-mounted nodes were used—one functioning as the transmitter and the other as the receiver, as described in 3.2.1.

A Samsung S23+ smartphone torch served as the light emitter, emulating a reflected sunlight beam to provide a stable optical carrier for modulation. Both the transmitter and receiver circuits were connected to a Keysight DSOX1102G oscilloscope on separate channels: one monitoring the 5V LCD modulation signal, and the other capturing the filtered output from the photodiode amplifier. Each channel was configured for DC coupling, with the voltage scale adjusted accordingly to the signal amplitude observed at the transmitter and receiver outputs. This allowed for a direct comparison between the transmitted and received waveforms, enabling analysis of signal attenuation, distortion, and timing behaviour through the optical channel.

To quantify ambient illumination conditions during testing, a free Lux meter Android application on the Samsung S23+ was used. The receiver-side microcontroller was not utilized during these experiments, as waveform analysis was conducted entirely through the oscilloscope.

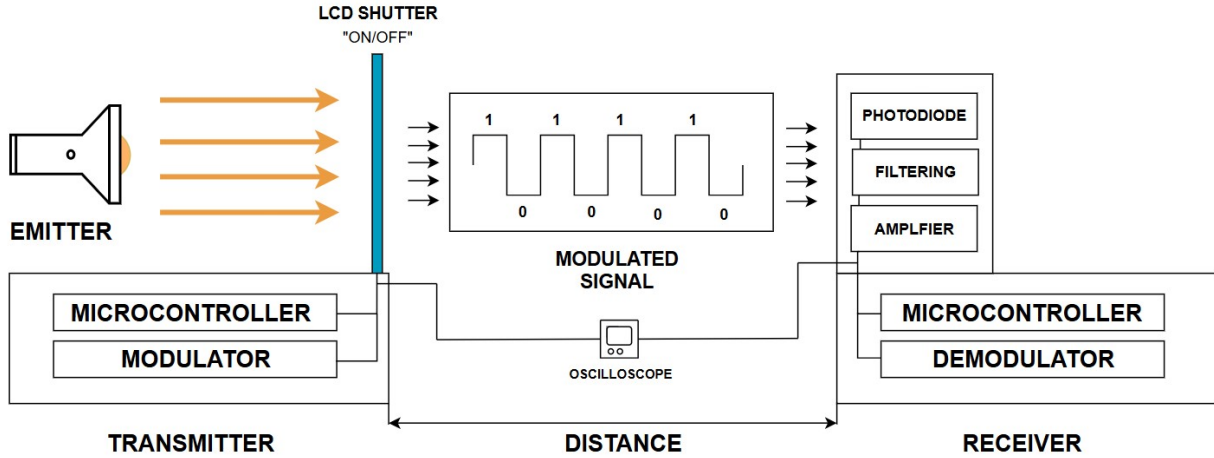


Figure 4: Communication subsystem block diagram.

3.2.3 Test Methods and Environment Conditions

A series of tests were performed under varying lighting conditions and distances to evaluate the communication subsystem's performance and robustness. Two lighting environments were used:

- Low-light condition: A dark room with minimal ambient illumination (15 lux).
- Ambient-light condition: A laboratory with fluorescent lighting off but several large windows admitting natural, overcast daylight (650 lux).

The ambient-light scenario was intended to approximate real outdoor conditions, though overcast weather and tinted windows reduced light intensity compared to a sunny day. Full outdoor testing was not conducted due to the impracticality of relocating the laboratory setup, however, the indoor ambient-light tests were considered sufficiently representative for performance evaluation.

For each test, the character 'A' (binary 1000001 in ASCII) was transmitted, as it includes both binary 1 and binary 0 transitions, thereby demonstrating both modulation frequencies with 5-bit repetition. Measurements were taken at four distances: 0.2 m, 0.5 m, 1.0 m, and 1.5 m, measured between the LCD transmitter and the photodiode receiver. The spacing between the LCD and the light source was negligible and remained constant throughout all trials. An additional measurement was taken in idle state for each lighting condition, (i.e. no transmission) to measure the pure noise signal introduced by the receiver circuitry.

4 RESULTS

4.1 Dynamic Sun-Tracking Subsystem

This subsection presents the results obtained from testing the dynamic sun-tracking subsystem under various conditions.

4.1.1 Light Sensing Array

Figure 5 shows the voltages measured at the MSP430 ADC for both the photodiodes and LDRs as a function of the sensor's angular position relative to the fixed LED light source. The plots indicate that the photodiode voltages decrease as the angular distance from the direct line of sight increases. The LDR array voltages exhibit greater variability, as shown by the less uniform shape of the LRD line, while the photodiodes register slightly higher voltages at the 10% light intensity level. For all light levels except the 10% case, both the LDR and photodiode outputs plateaued at approximately 5 V between 60° and 210°. In the 10% illumination test, the plateau occurred between 90° and 180°.

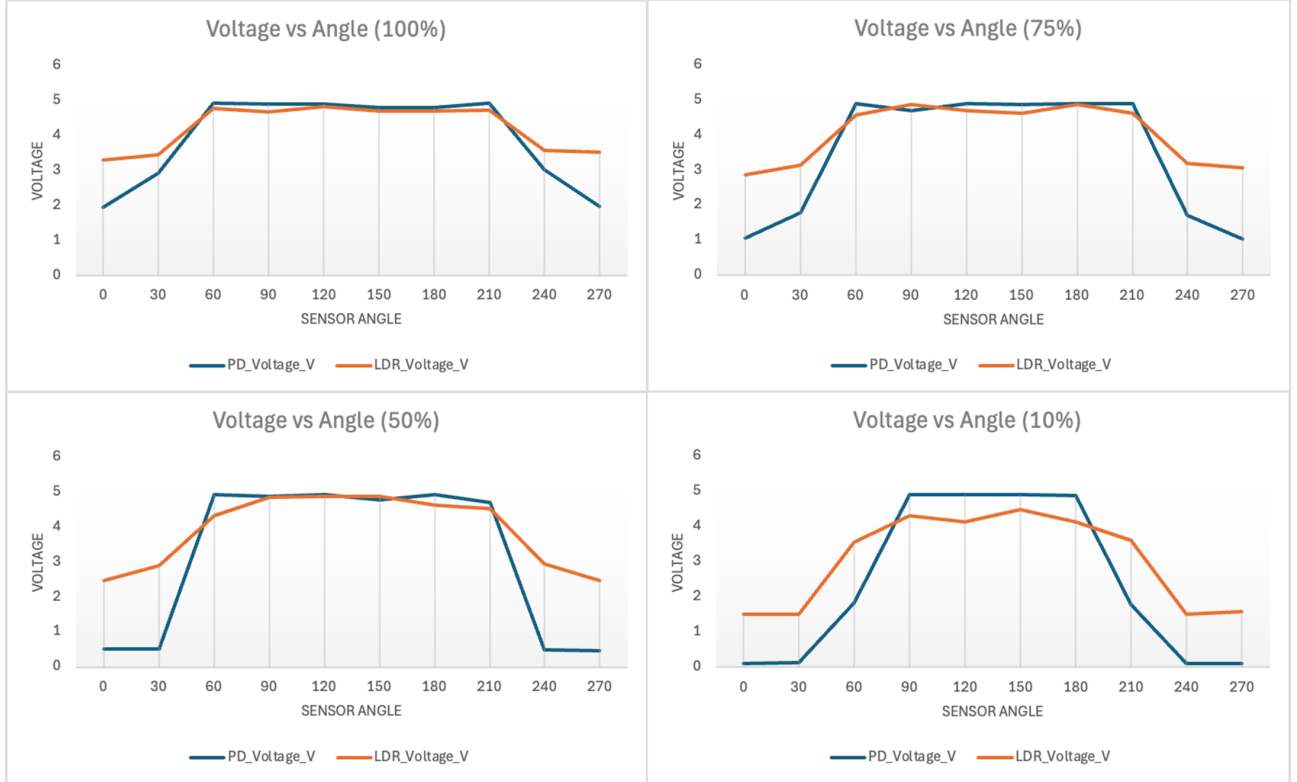


Figure 5: Voltage versus angular position for the light-sensing array at four illumination levels: 100% (top left), 75% (top right), 50% (bottom left), and 10% (bottom right). PD_Voltage_V represents the measured photodiode voltage, and LDR_Voltage_V represents the measured LDR array voltage.

Figure 6 shows the illumination in Lux for the previous set of results at each of the varied brightness levels.



Figure 6: Graph showing the illumination levels in Lux vs angle of sensor for the 10%, 50%, 75% and 100% light levels used in the experiment.

4.1.2 Motor Circuit

The initial LTSpice simulation result for the NEMA 17 stepper motor, shown in Figure X, indicates a sharp current rise to approximately 1.4A at the moment the step input is applied, before settling to around 88mA in the idle state.

The results for the experiments performed on the motor can be seen in Table 1, providing a comparison between measured values and those obtained from LTSpice simulations.

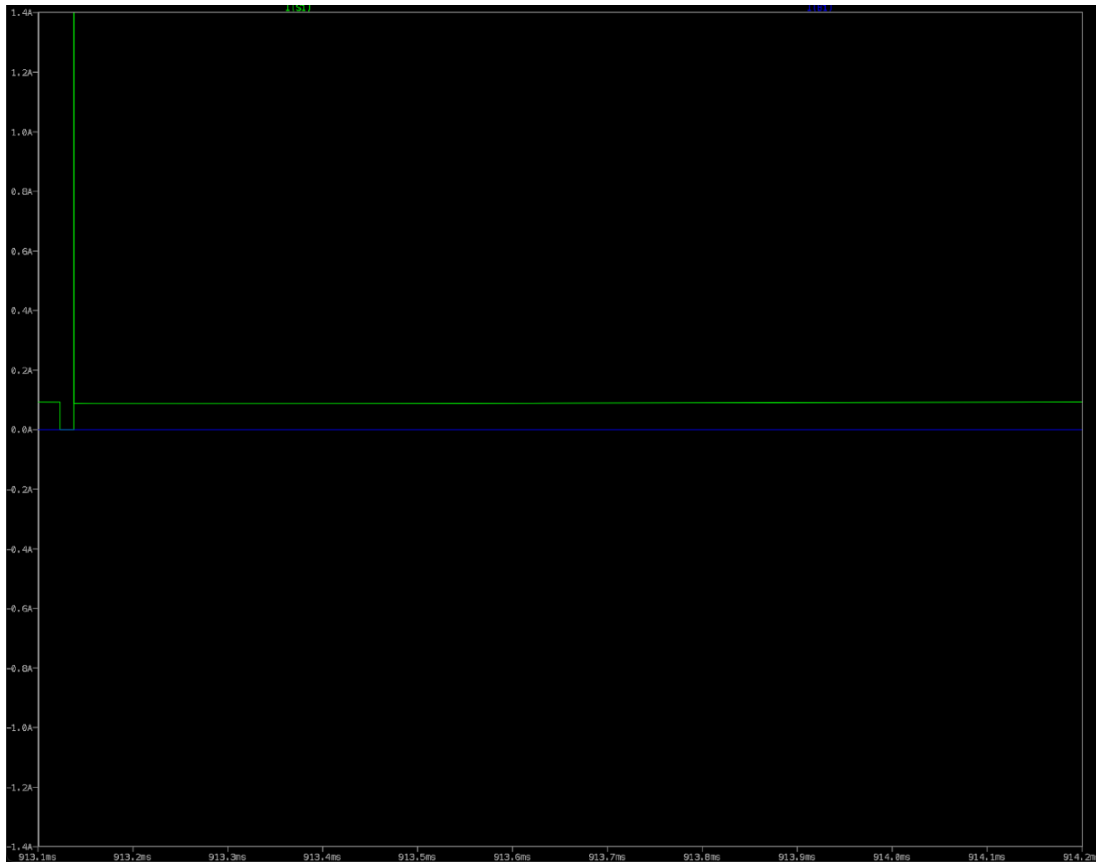


Figure 7: LTSpice simulation result for the NEMA 17 stepper motor showing current response to an applied step input signal.

Parameter	Measured	Simulated
Supply Voltage	11.76V	11.90V
Coil Voltage Drop	3.357V (per phase)	3.88V (per phase)
Supply Current	1.325A	1.3A
Motor Back-EMF	0.789V	0.81V
PWM Switching Frequency	19.87kHz	20.2kHz
Idle (no step)	0.015V	0.02V
Full Step (single step)	0.267V	0.356V
Step to Desired Location (0–90°)	1.2653V, 0.8143A	1.1469V, 0.8211A
Step to Desired Location (0–180°)	4.5432V, 0.9578A	4.5651V, 0.9654A
Step to Desired Location (0–270°)	10.0871V, 1.2245A	10.42V, 1.2891A

Table 1: Summary of measured results from the experiments performed on the motor. Note that the voltages and currents stated in the bottom three rows (covering the 0–270° sweep) are averages for both the measured and simulated results.

4.2 Communication Subsystem

This subsection presents the results obtained from testing the communication subsystem under various conditions. In all figures presented, Signal 1 (dark blue) corresponds to the transmitted waveform, while Signal 2 (purple) represents the received waveform at the photodiode output.

4.2.1 Pure Noise Signal

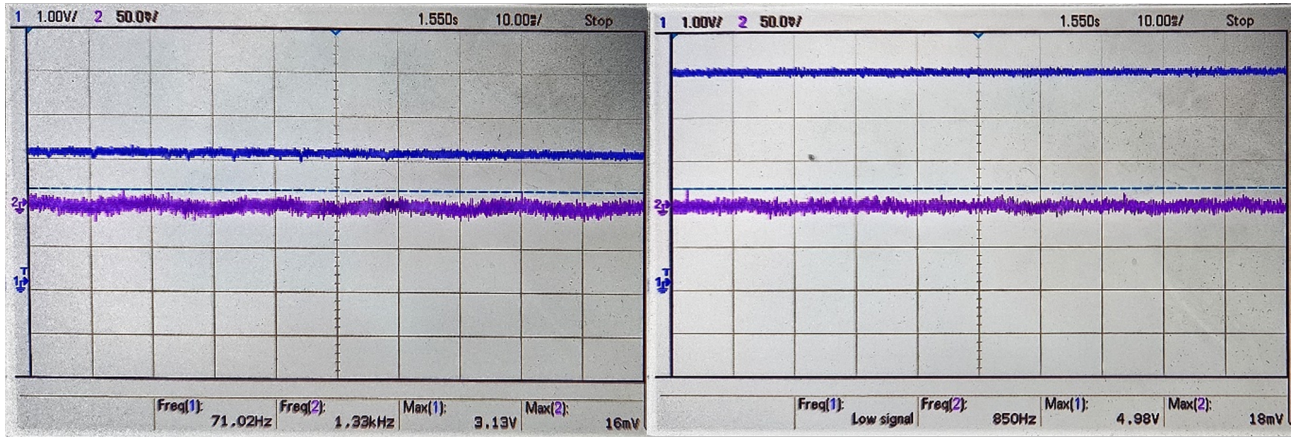


Figure 8: Oscilloscope output for pure noise signal, in (left) daylight ambient conditions and (right) dark light conditions.

4.2.2 Distance 0.2m

At a separation distance of 0.2m, the received waveforms under both daylight and dark conditions closely match the transmitted signal, demonstrating successful optical modulation and detection. As shown in Figure 4.3, the oscilloscope vertical scale differs between the two conditions—500 mV/div for the dark environment and 100 mV/div for the ambient daylight condition. This difference causes the daylight signal to appear larger and clearer in the figure, despite the measured peak amplitude being higher in the dark environment (453 mV) compared to the daylight condition (221 mV).

4.2.3 Distance 0.5m

At a distance of 0.5m, the oscilloscope voltage scale was set to 50 mV per division for both ambient daylight and dark conditions (Figure 4.4). The received signal quality shows a significant reduction compared to the 0.2 m tests, with peak amplitudes decreasing from 221 mV to 62 mV under daylight and from 453 mV to 119 mV under dark conditions. Additionally, the received waveforms exhibit increased noise, evident from their more irregular shape compared to the clearer signals observed at shorter range.

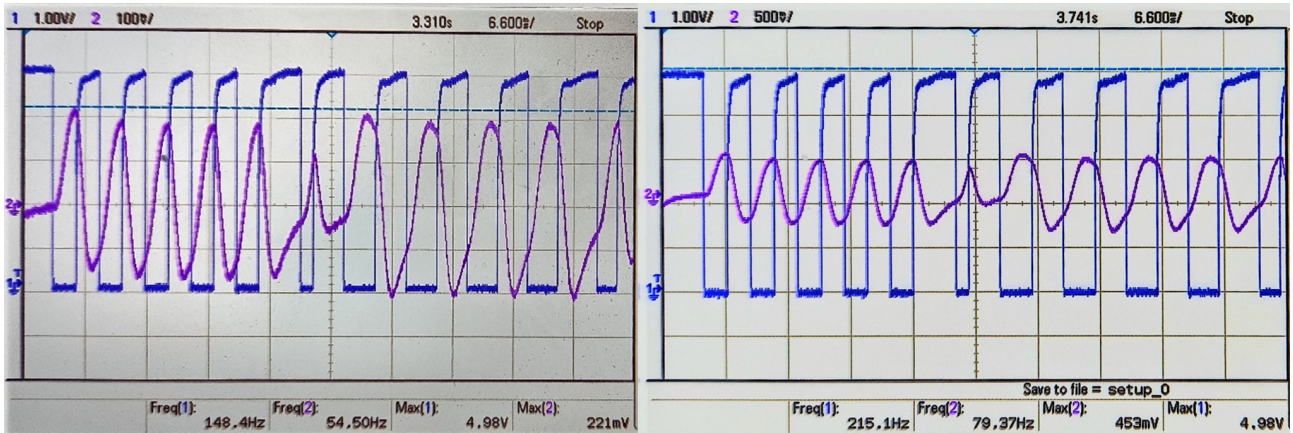


Figure 9: Oscilloscope output for measurement taken at 0.2m, in (left) daylight ambient conditions and (right) dark light conditions.

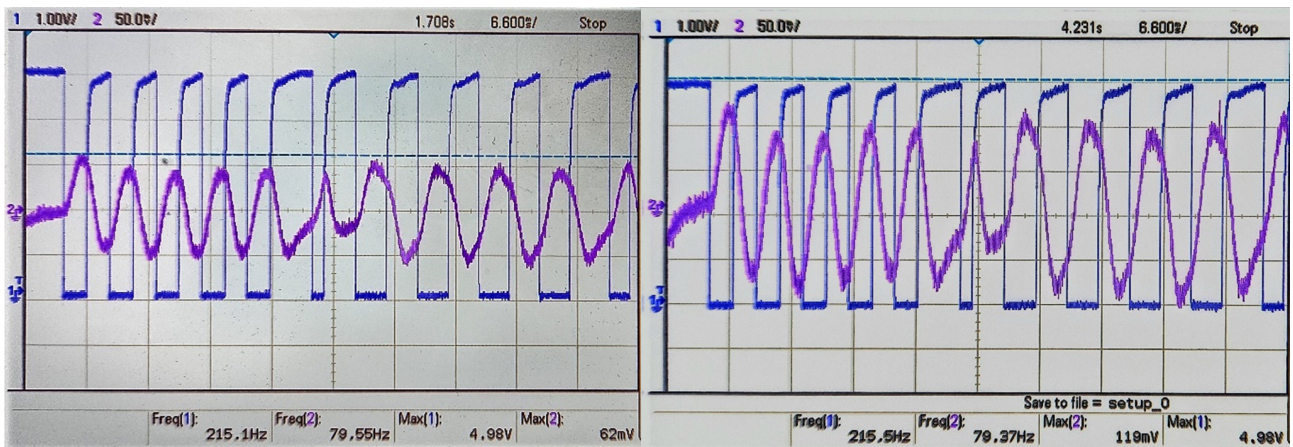


Figure 10: Oscilloscope output for measurement taken at 0.5m, in (left) daylight ambient conditions and (right) dark light conditions.

4.2.4 Distance 1.0m

At a separation distance of 1.0 m between the LCD and the receiving circuit, the received signals for both lighting conditions are shown in Figure 4.5. The peak voltages measured were 24 mV under ambient daylight and 35 mV under dark conditions. Although the received waveforms exhibit increased background noise relative to the signal, the transmitted modulation remains visible within the captured traces.

4.2.5 Distance 1.5m

At a distance of 1.5 m, the communication subsystem reached the maximum range achievable under ambient daylight conditions. As shown in Figure 4.6, the peak voltages of the received signals were 16 mV for daylight and 27 mV for dark conditions. The signal-to-noise ratio decreased noticeably compared to the 1.0 m measurements. For the daylight condition, the peak voltage is approximately equal to the baseline noise level recorded in Figure 4.2, indicating the experimental maximum range under these lighting conditions.

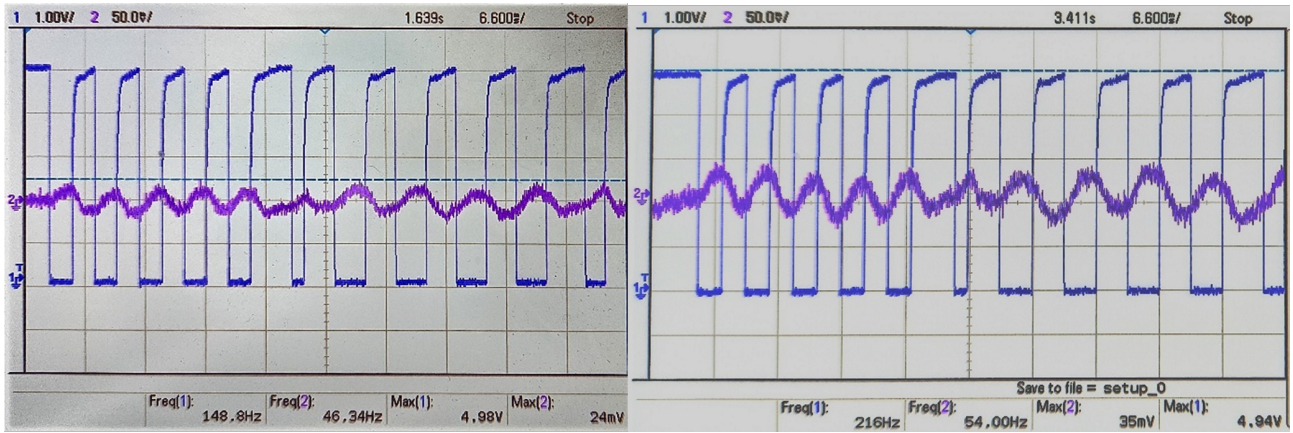


Figure 11: Oscilloscope output for measurement taken at 1.0m, in (left) daylight ambient conditions and (right) dark light conditions.

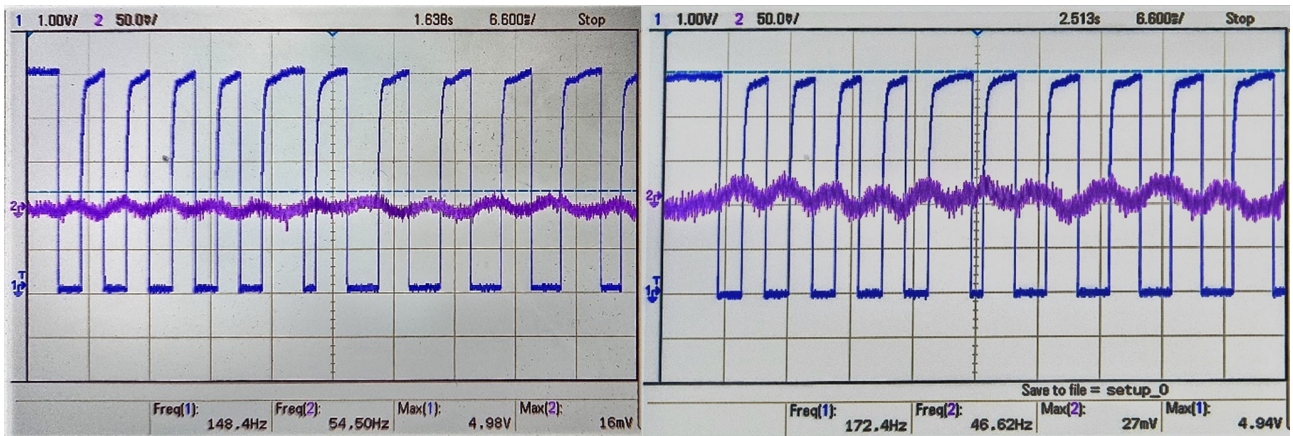


Figure 12: Oscilloscope output for measurement taken at 1.5m, in (left) daylight ambient conditions and (right) dark light conditions.

4.2.6 Graphs

Figure 13 shows the measured voltages plotted against distance. The graphs indicate an exponential decrease in peak voltage as the distance between the transmitter and receiver is increased under both lighting conditions. Additionally, the measured voltages under ambient light are consistently lower than those observed in dark conditions.

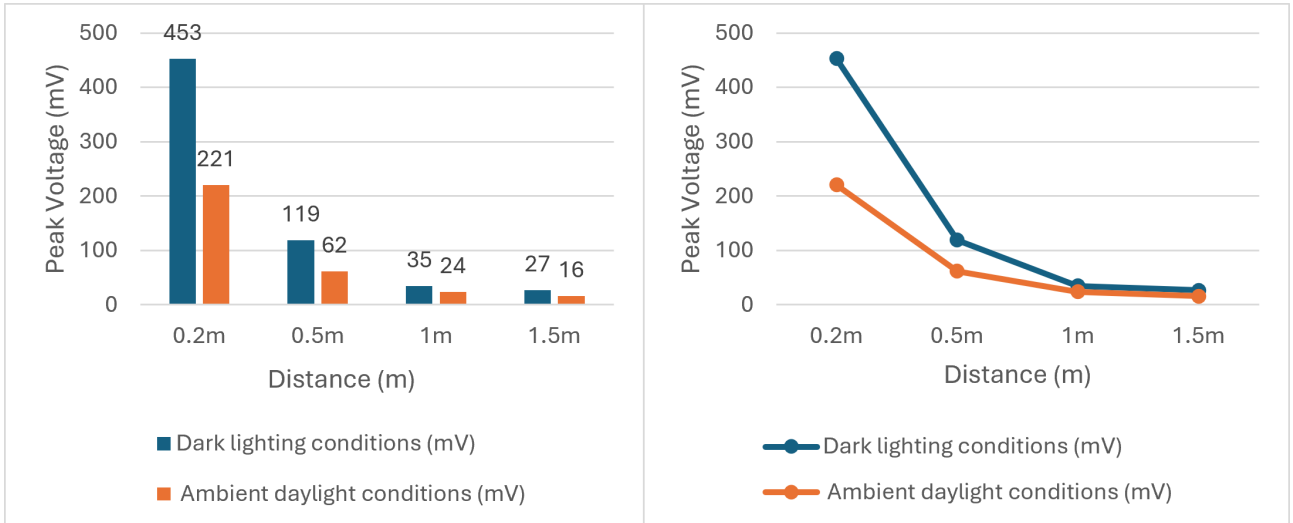


Figure 13: Bar graph showing decreasing maximum voltage with increased distance (left) and line graph showing downward trend with increased distance (right) .

It's also to note that flickering was observed at the LCD during transmission.

5 DISCUSSIONS

5.1 Light Sensing Array

The light sensing array demonstrated potential for accurately tracking a variable light source. However, the results indicate clear oversaturation, particularly for the photodiodes, which remained at maximum voltage across roughly 60% of the 270° angular range for the 100%, 75%, and 50% illumination levels, and around 40% of the range for the 10% test. Considering the measured illuminance values, with the 100% level corresponding to approximately 4.6 kLux, it is evident that under real sunlight conditions (ranging from 10 to 100 kLux) the light array in its current form would likely saturate across an even broader angular range. Oversaturation would result in minimal differential voltage input to the PI controller, potentially preventing the motor from initiating movement and compromising the system's ability to track the sun effectively.

The combination of LDRs for coarse directional sensing and photodiodes for fine-tuned detection enhances overall accuracy. The LDRs respond to light over a broader angular range, capturing the general direction of the source, whereas the photodiodes exhibit greater sensitivity over narrower angles, supporting precision adjustments. Based on the ADC measurements recorded during the experiments, it can be reasonably assumed that, with full integration between the light sensing array and motor control circuitry, the system would successfully track a moving light source across the sky. It is important to note that the tests were performed using an artificial LED source, which is more directional and stable than sunlight. In real-world con-

ditions, additional factors such as diffuse sunlight, glare, and dynamic environmental changes could introduce interference, potentially reducing tracking accuracy. This may manifest as the system correcting too frequently or too little depending on the ambient light variability, highlighting the need for further refinement in sensor calibration and controller tuning to maintain reliable performance under natural sunlight conditions.

5.2 Motor Application

The experimental results for the azimuth motor indicate that, although tracking the sun could improve signal quality for a light-based communication system, the overall power consumption is unreasonably high compared to the benefits. Even for a small step rotation (0–90°), the measured average voltage and current were 1.2653V and 0.8143A, respectively, corresponding to an approximate power draw of 1W ($P = IV$). By comparison, existing ambient light systems, such as PassiveVLC, operate at micro-watt power levels [8], highlighting a difference of several orders of magnitude. For context, 1 Watt is one million times greater than a micro-Watt, illustrating the substantial energy cost of motorized sun tracking. It is also important to note that the measured 1W draw does not account for the additional weight of transceiver components that would be mounted on the motor, which would inevitably increase power consumption. Furthermore, while experiments were not conducted on the elevation motor, which were deemed unnecessary due to the directional illumination applied during testing, full sun tracking in a real environment would require multi-axis control to follow the sun’s path across the sky. Incorporating an elevation motor would therefore further increase energy requirements.

From a system feasibility perspective, the use of a 12V supply to drive the motor is impractical for low-power, remote IoT devices, which would require voltage conversion or regulation. Although the motor can technically operate at lower voltages (e.g. 5 V), this reduces available torque and can reduce the accuracy of the stepping control, further limiting performance. Overall, while the concept of motorized sun tracking is novel, the high power requirements and practical constraints make it unsuitable for low-power IoT applications in its current form.

5.3 Communication System

The communication subsystem results aligned broadly with expectations based on prior research and the known characteristics of light detection circuitry - as distance increases, the received light signal decreases exponentially [6]. Some flickering was observed, despite the frequencies selected being above the visual threshold, which is likely attributable to the discrete pulse-based FSK introduced by the 5-bit repetition scheme. While the subsystem design shares similarities with the LuxLink project, which achieved an operational range of 4–60m in ambient light conditions [9], the experimental setup here only achieved a maximum range of 1.5m. Several

design differences explain this disparity: LuxLink employed a continuous FSK modulation scheme, utilized higher carrier frequencies (560 Hz and 640 Hz) compared to the 170 Hz and 230 Hz used here, and relied on reflected sunlight as the emission source, which is inherently stronger and contains more energy than the Samsung S23+ phone torch used for testing in this project. Additionally, this project did not implement message decoding. Instead, the maximum operating distance was estimated based on the point at which the signal-to-noise ratio approached unity. In contrast, LuxLink leveraged a Fast Fourier Transform (FFT) to decode the signal in the frequency domain, allowing for effective noise filtering and reconstruction of the transmitted waveform.

Considering these factors, the most impactful difference is likely the light source. A stronger illumination source, such as sunlight, provides a more robust medium for data transmission, improving range and signal integrity. The next most significant factor is the use of FFT decoding, which enables signal recovery even under noisy conditions. Even in the experiments conducted here, the received signal at 1.5 m still exhibited discernible modulation that loosely followed the transmitted waveform, suggesting that with a continuous FSK scheme and FFT-based decoding, the system could potentially achieve higher operational ranges.

An additional issue discovered during the experiments was a perceptible flickering at the LCD during transmission. Adjusting the carrier frequencies to be well above the human visual range would likely reduce flickering further, which, while not critical for remote IoT applications, remains important to consider for environmental impact, particularly on wildlife sensitive to low-frequency light modulation.

Overall, the results highlight that both the illumination source and the decoding methodology are key determinants of performance for low-power visible light communication systems. In terms of the general feasibility of the communication system, further research and modifications would be required to increase the operational range. In its current place, deploying a receiver every 1.5m would not be practical or cost-effective for real-world applications.

6 CONCLUSIONS

This research set out to design and prototype a communication system that utilises sunlight as a medium for backscattered communication, incorporating dynamic sun tracking to maximise signal reliability. The results demonstrate that while the concept is feasible, several practical limitations currently restrict its performance and scalability in low-power IoT contexts.

The light sensing array showed clear potential for accurate light source detection and tracking, with the combined use of LDRs and photodiodes offering both coarse and fine angular resolution. However, oversaturation of the photodiodes across up to 60% of the angular range under moderate illumination levels (approximately 4.6 kLux) suggests that, under real sunlight conditions, differential sensing would be severely limited in its current state. This would likely reduce the precision of the PI controller and impair the ability of the motor to continuously track the sun, particularly under varying lighting conditions.

Motor testing revealed that the azimuth control consumed an average of approximately 1W (1.2653 V, 0.8143 A) for small-step movements, which is several orders of magnitude greater than the micro-watt power levels existing ambient light systems such as PassiveVLC achieve. The requirement for a 12 V supply and potential inclusion of an additional motor covering the elevation axis would further increase energy consumption, making motorised tracking impractical for low-power, IoT nodes. These results highlight the challenge of balancing dynamic light alignment with strict energy constraints.

The communication subsystem achieved a maximum operational range of 1.5m under ambient indoor lighting using a smartphone torch as the illumination source. While this demonstrated data transmission using ambient light, the range fell well short of similar systems, such as LuxLink, which achieved 4–60 m using sunlight and continuous FSK modulation. The key limiting factors identified were the relatively weak artificial light source and the absence of FFT-based signal decoding. Despite this, the observed signal patterns suggest that adopting continuous modulation and frequency-domain decoding could substantially improve range and robustness.

Overall, the research demonstrates the potential of leveraging ambient light as a sustainable medium for ultra-low-power IoT networks, reinforcing the importance of continued investigation into more efficient modulation, decoding, and tracking strategies to enable long-range, low-energy optical communication in outdoor environments.

7 RECOMMENDATIONS FOR FUTURE WORKS

For the sunlight tracking subsystem, future improvements should focus on refining the sensor array and reducing overall power consumption. Modifying the sensor surface to adopt a more curved geometry could enable a semi-passive tracking approach, allowing the system to maintain alignment with minimal motor intervention. Additionally, exploring smaller, low-torque motors would help reduce current and voltage spikes, significantly lowering the system's power profile and making it more suitable for low-power IoT applications.

For the communication subsystem, several key enhancements could substantially improve performance. Implementing continuous FSK modulation would eliminate flickering and produce a more stable transmission. Integrating FFT-based message decoding would likely extend the operational range beyond the 1.5 m achieved in this work by enabling more robust signal recovery in noisy conditions. Finally, future experiments should utilise a stronger light source such as direct sunlight, to better reflect real-world operating environments and improve the overall signal strength and reliability of the system.

References

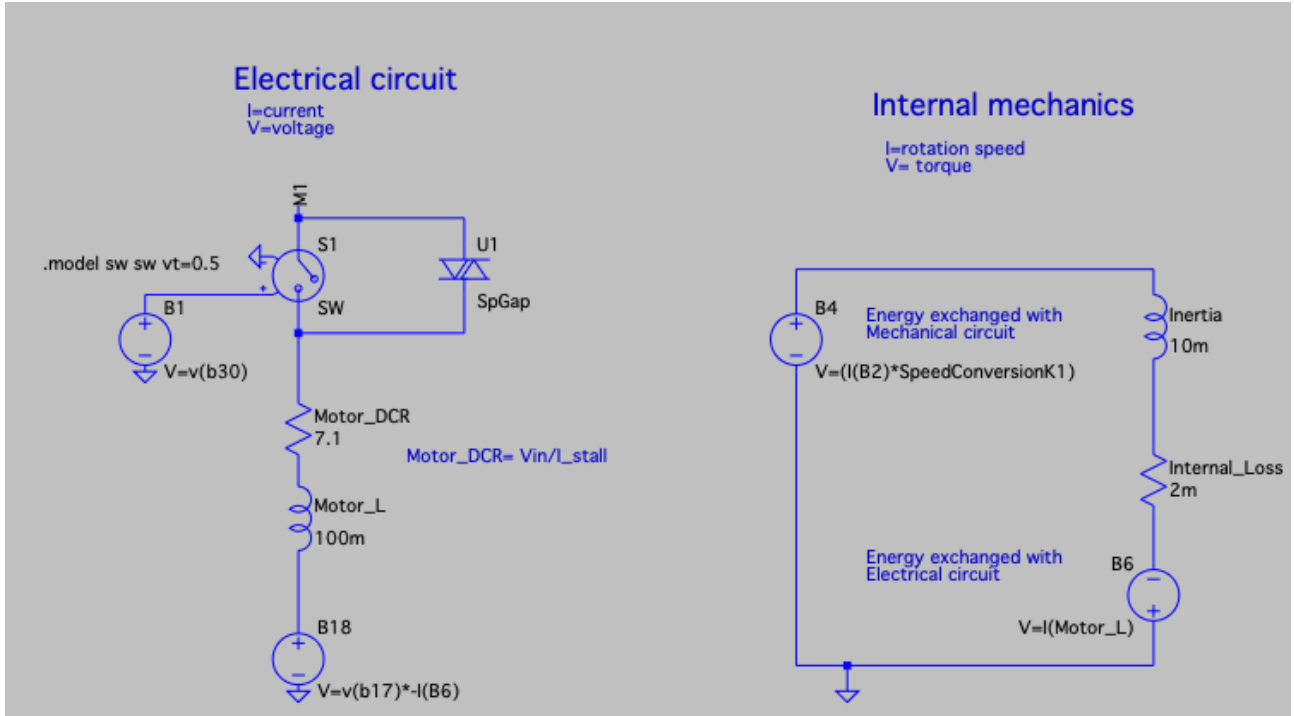
- [1] History of Radio, Wikipedia, Feb. 3, 2019. [Online]. Available: https://en.wikipedia.org/wiki/History_of_radio
- [2] H. Haas, L. Yin, Y. Wang, and C. Chen, "What is LiFi?" *Journal of Lightwave Technology*, vol. 34, no. 6, pp. 1533–1544, 2016, doi: 10.1109/JLT.2015.2510021.
- [3] Radio Spectrum Management, "Radio Spectrum Allocation Chart - New Zealand," 2024. [Online]. Available: <https://www.rsm.govt.nz>, Accessed: Apr. 3, 2024.
- [4] A. A. Irudayaraj and A. S. Nittala, "LightLink: Enhancing Smartwatch Sensing and Actuation Through Visible Light Communication," in *Proc. 38th Annual ACM Symposium on User Interface Software and Technology (UIST '25)*, 2025, article no. 190, pp. 1–18, doi: 10.1145/3746059.3747623.
- [5] L. E. M. Matheus, A. B. Vieira, L. F. M. Vieira, M. A. M. Vieira, and O. Gnawali, "Visible Light Communication: Concepts, Applications and Challenges," *IEEE Communications Surveys & Tutorials*, vol. 21, no. 4, pp. 3204–3237, Fourthquarter 2019, doi: 10.1109/COMST.2019.2913348.
- [6] Q. Wang, M. Zuniga, and D. Giustiniano, "Passive Communication with Ambient Light," in *Proc. 12th International Conference on emerging Networking EXperiments and Technologies (CoNEXT '16)*, New York, NY, USA, 2016, pp. 97–104, doi: 10.1145/2999572.2999584.
- [7] P. Wang, L. Feng, G. Chen, C. Xu, Y. Wu, K. Xu, G. Shen, K. Du, G. Huang, and X. Liu, "Renovating road signs for infrastructure-to-vehicle networking," in *Proc. 26th Annual International Conference on Mobile Computing and Networking*, 2020, doi: 10.1145/3372224.3380883.
- [8] X. Xu, Y. Shen, J. Yang, C. Xu, G. Shen, G. Chen, and Y. Ni, "PassiveVLC: Enabling Practical Visible Light Backscatter Communication for Battery-free IoT Applications," in *Proc. 2017 ACM Int. Conf. on Mobile Computing and Networking (MobiCom '17)*, Snowbird, UT, USA, 2017, pp. 175–186, doi: 10.1145/3117811.3117843.
- [9] R. Bloom, M. Z. Zamalloa, and C. Pai, "LuxLink: creating a wireless link from ambient light," 2019, doi: 10.1145/3356250.3360021.
- [10] M. A. Chávez Tapia, T. Xu, and M. Zúñiga Zamalloa, "Sol-Fi: Enabling Ultra-Low-Power Wireless Communication with Solar-Powered Internet of Things Devices," in *Proc. 2024 IEEE/ACM Int. Conf. on Information Processing in Sensor Networks (IPSN)*, San Diego,

CA, USA, 2024, pp. 1–10, doi: 10.1109/IPSN61024.2024.00010.

- [11] S. K. Ghiasi, M. Kaldenbach, and M. Zuniga, "Passive Screen-to-Camera Communication," in *2024 20th Int. Conf. on Distributed Computing in Smart Systems and the Internet of Things (DCOSS-IoT)*, 2024, pp. 35–43, doi: 10.1109/dcoss-iot61029.2024.00016.

Appendices

A Sun-Tracking Subsystem LTSpice Models



The LTSpice model of the NEMA 17 stepper motor is divided into an electrical circuit (left) and internal mechanical components (right).

Electrical Circuit:

- **B1 – Control/Ramp Source:** Drives the voltage-controlled switch.
- **S1 / SW – Voltage-Controlled Switch:** Connects or disconnects the motor winding.
- **U1 – Diode:** Provides a flyback/recirculation path for winding current when S1 opens, capturing the inductive kick.
- **Motor_DCR – Winding Resistance:** Represents the copper resistance of the winding.
- **Motor_L – Winding Inductance (100 mH):** Models the inductive characteristics of the winding.

Internal Mechanical Components:

- **B6 – Torque Source:** Converts electrical input to mechanical torque.
- **Inertia (10 m):** Represents rotor inertia, converting torque into rotational speed.
- **Internal Loss (Friction Losses):** Models damping according to motor specifications.
- **B4 – Back EMF Term:** Simulates the voltage generated by rotor motion opposing the applied voltage.

This model allows simulation of both electrical motor behavior under step inputs, enabling comparison with measured voltage and current responses.